ADVANCED FUNCTIONAL MATERIALS
www.afm-journal.de

Nature of Charge Carriers in a High Electron Mobility Naphthalenediimide Based Semiconducting Copolymer

Valerio D'Innocenzo, Alessandro Luzio, Annamaria Petrozza, Daniele Fazzi, and Mario Caironi**

The nature of charge carriers in recently developed high mobility semiconducting donor-acceptor polymers is debated. Here, localization due to charge relaxation is investigated in a prototypal system, a good electron transporting naphthalenediimide based copolymer, by means of current-voltage *I–V* electrical characteristics and charge modulation spectroscopy (CMS) in top-gate field-effect transistors (FETs), combined with density functional theory (DFT) and time dependent DFT (TDDFT) calculations. In particular, pristine copolymer films are compared with films that underwent a melt-annealing process, the latter leading to a drastic change of the microstructure. Despite the packing modification, which involves also the channel region, both the electron mobility and the energy of polaronic transitions are substantially unchanged upon melt-annealing. The polaron absorption features can be rationalized and reproduced by TDDFT calculations for isolated charged oligomers. Therefore, it is concluded that in such a high electron mobility copolymer the charge transport process involves polaronic species which are intramolecular in nature and, from a more general point of view, that interchain delocalization of the polaron is not necessary to sustain charge mobilities in the 0.1 to 1 $cm^2 V^{-1} s^{-1}$ range. These findings contribute to the rationalization of the charge transport process in the recently developed class of donor-acceptor π-conjugated copolymers featuring high charge mobilities and complex morphologies.

1. Introduction

Understanding the nature of charge carriers and their transport mechanisms[1–4] in organic semiconductors is of utmost importance to design materials with optimized properties for future organic electronic and clean energy applications.[5–8] Huge efforts have been spent in the last decades to investigate the chemical-physical mechanisms governing charge transport in both small molecules and polymer thin films. As a result, efficient design rules and guidelines emerged to optimize the chemical structure, film morphology, and eventually charge carrier mobility.[7,9–11]

Organic field-effect transistors (OFETs)[12] can be seen both as ideal tools to study transport in thin channels where the charge density can be electrostatically controlled, typically in the range of 10^{18}–10^{19} cm^{-3}, and as fundamental building blocks for the development of organic electronic circuits.[13,14] In this device the understanding of the physical mechanism leading to an improved field-effect mobility μ has a direct technological importance.

While a band-like transport has been observed in OFETs based on ultrapure single crystals[15,16] and highly ordered films based on small molecules,[17,18] so far only a thermal activated transport regime has been reported in the case of semiconducting polymers. Thermal barriers to transport may arise either from charge relaxation, e.g., polaronic effects[19,20] or from an inherently higher degree of static disorder,[21] which characterizes most of the conjugated polymer films. Nevertheless, carriers mobilities in the 0.1 to 10 $cm^2 V^{-1} s^{-1}$ range were demonstrated even in simply spin-cast films lacking strong long range order, as in the case of the recent generation of donor-acceptor copolymers.[22] While such charge mobility values are making real applications of organic electronics a closer opportunity, they even more urge for deeper theoretical and experimental investigations to clarify the nature of the charge carrier and the energetic landscape it experiences during the transport process. The previously adopted paradigm that guided the development of increasingly ordered films, from poly(3-hexylthiophene)[23] to interdigitated poly[5,5′-bis(3-alkyl-2-thienyl)-2,2′-bithiophene] (PQT) and poly[2,5-bis(3-alkylthiophene-2-yl)thieno(3,2-b)thiophene] (pBTTT),[24–26] appears not to be general enough to explain recent observations. Various models have and are being debated to properly describe charge transport, from hopping to mobility edge mechanisms.[21,27–33] While these models can be generally used to fit experimental data, they find justification in completely different physical

V. D'Innocenzo, A. Luzio, A. Petrozza, M. Caironi
Center for Nano Science and Technology @PoliMi
Istituto Italiano di Tecnologia
Via Giovanni Pascoli 70/3
20133, Milan, Italy
E-mail: mario.caironi@iit.it
V. D'Innocenzo
Dipartimento di Fisica
Politecnico di Milano
Piazza L. da Vinci, 32
20133, Milano, Italy
D. Fazzi
Max-Planck Institut für Kohlenforschung
Kaiser-Wilhelm-Platz 1
D-45470, Mülheim an der Ruhr, Germany
E-mail: fazzi@mpi-muelheim.mpg.de

DOI: 10.1002/adfm.201400394

scenarios. Recently a unifying picture for charge transport in polymers has been proposed.[34] In this model the lattice disorder in short-range molecular aggregates, efficiently interconnected through tie-molecules, limits the carrier mobility over the long range,[34] and charge transport is described in a multiple trap and release fashion due to a tail of localized electronic states controlled by lattice paracristallinity. In parallel, other works are reporting the effect of long-range orientational order on the field-effect mobility of high mobility polymer devices,[22,35] and quasi-1 dimensional transport along rigid polymer backbones with efficient π-stacked regions, limiting inter-chain jumps.[36] In this frame, to achieve a clear view over charge transport for the new copolymer generation and to propose reliable parameters for quantitative models,[37] it is important to shed light on the nature of charge carriers, and in particular on the extent of their spatial extension (both intra- and intermolecular).

With this contribution, we aim to clarify the above mentioned point in an exemplary electron transporting material, poly{[*N*,*N*′-bis(2-octyldodecyl)-naphthalene-1,4,5,8-bis(dicarboximide)-2,6-diyl]-alt-5,5′-(2,2′-bithiophene)}, P(NDI2ODT2), an n-type semiconducting copolymer showing an electron field-effect mobility exceeding 1 $cm^2\ V^{-1}\ s^{-1}$.[22,38] We adopt a combined experimental and theoretical approach to investigate charge relaxation effects in films subjected to profound, thermal-induced, structural modifications: the investigation is performed by means of charge modulation spectroscopy (CMS), a technique capable of probing charge-induced spectral features in the channel of a working OFET,[2,19,23,39] density functional theory (DFT), and time dependent DFT (TDDFT) calculations to accurately compute the electronic structures, transitions, and absorption spectra of both neutral and charged polymer species. Our results show that charge-induced absorption features identified in the CMS spectra closely resemble the optical transitions belonging to the charged isolated polymer segment, as revealed by TDDFT calculations. This observation identifies clear polaronic effects, where the extra charge is substantially confined intra-molecularly on few repeat units of a single P(NDI2OD-T2) chain. Moreover, thermally induced structural modifications do not affect the electron mobility as well as the energy of the main CMS absorption. Our investigation therefore clarifies that in high electron mobility copolymers, such as P(NDI2OD-T2), inter-chain polaron delocalization is not a necessary condition to achieve a field-effect mobility in the 0.1–1 $cm^2\ V^{-1}\ s^{-1}$ range.

2. Results and Discussion

In order to study the nature of charge carriers in P(NDI2OD-T2), we have investigated and compared both pristine films, namely films subjected to a mild thermal treatment only (e.g., 120 °C in N_2 atmosphere), and melt-annealed films, which have undergone a slow melting and cooling process, known to strongly affect their microstructure[40–43] (see Section 4 for details on film preparation). Films have been characterized by UV-Vis absorption spectroscopy, and by electrical and CMS measurements when integrated in OFET devices, as described in the next section, where spectroscopic experimental data are discussed together with DFT and TDDFT calculations.

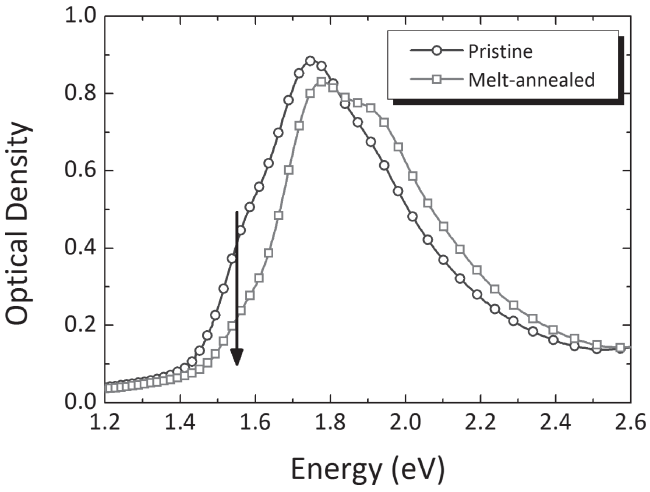

Figure 1. UV-Vis absorption spectra of P(NDI2OD-T2) before (circles) and after melt-annealing treatment (squares), normalized to the absorption peak centred at 3.1 eV (not shown here, see Supporting Information, Figure S2). The thermal treatment of the semiconducting layer labelled as pristine refers to an overnight annealing at 120 °C, while the melt-annealing treatment corresponds to an annealing at 350 °C with both heating and cooling rates of about 10 °C/min.

2.1. UV-Vis Absorption Spectra of Pristine and Melt-Annealed P(NDI2OD-T2) Films: Transition Assignment Through TDDFT Calculations on Neutral Species

The low energy region (1.2–2.6 eV) of the absorption spectra of P(NDI2OD-T2) thin films, before and after the melt-annealing process,[41] is reported in **Figure 1**. Both spectra show a broad absorption band with three distinct spectral features at 1.55 eV, 1.77 eV, and 1.90 eV, the relative intensity of which is altered by the melt-annealing treatment. According to previous literature[44,45] and based on quantum chemical calculations as reported below, we assign the band with a maximum at 1.77 eV to a charge transfer (CT) like excitation featuring a vibronic replica centred at 1.90 eV. The latter is more pronounced in the melt-annealed P(NDI2OD-T2) films. The low energy band (shoulder) at 1.55 eV, previously assigned by Steyrleuthner et al.[45] to an aggregate induced transition, drastically reduced its intensity upon melt-annealing, indicating a redistribution of the cross section due to a rearrangement of the packing motif of the polymer chains.

Further insights into the optical properties of highly oriented, epitaxially grown P(NDI2OD-T2) films have been reported by Brinkmann et al.[46] They isolated two distinct polymorphs characterized by a segregated stacking (called form I), where one naphthalenediimide (NDI2OD) (bithiophene, T2) unit faces another NDI2OD (T2) unit, and a mixed inter-chain stacking (form II), in which one NDI2OD (T2) unit faces a T2 (NDI2OD) unit. The absorption spectra of these remarkably ordered crystalline phases show similar band shapes as compared to the usual films deposited by spin-coating. In particular, the transition at 1.55 eV is more pronounced in the segregated phase than in the mixed inter-chain one. We therefore highlight a correspondence between the spectra collected on the pristine and melt-annealed P(NDI2OD-T2) films deposited by spin-coating

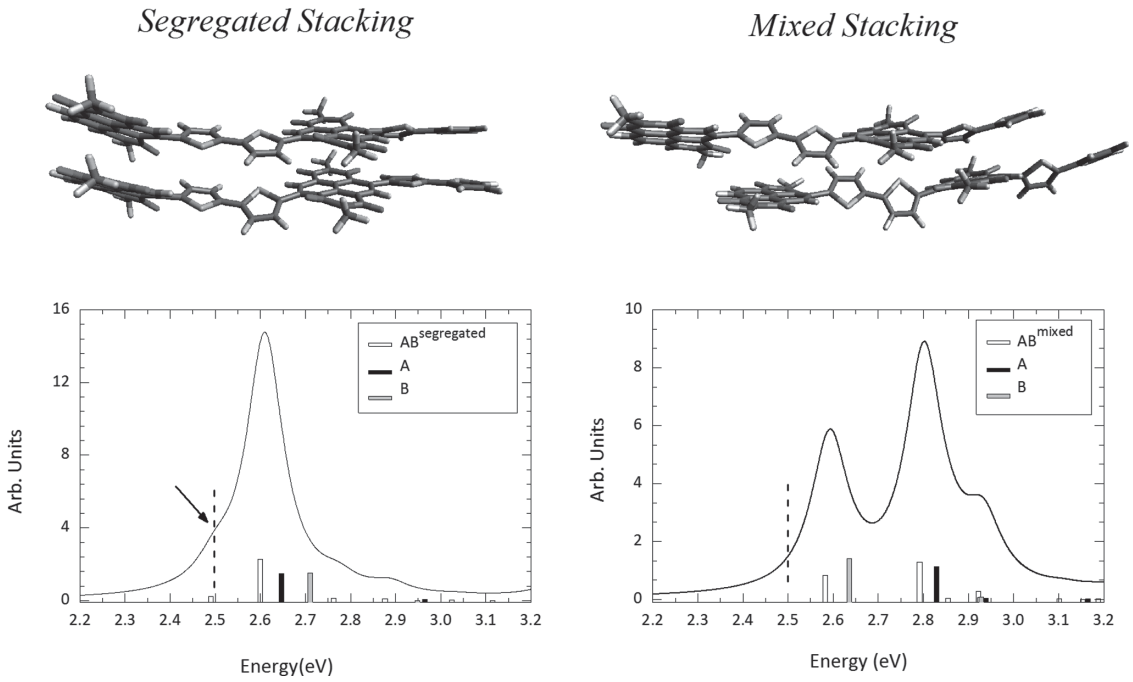

Figure 2. Upper panels: optimized DFT (ωB97XD/6–311G**) dimers of P(NDI2OD-T2) oligomers featuring a chain length of $n = 2$. Left side: segregated stacking with NDI2OD (T2) units facing NDI2OD (T2) units; right side: mixed stacking with NDI2OD (T2) units facing T2 (NDI2OD) units. Bottom panels: TDDFT (TD-ωB97XD/6–31G*) computed electronic transitions for both dimers (black lines (normalized spectra) and white sticks (oscillator strength), named $AB^{segregated}$ and AB^{mixed}) and for the single oligomers ($n = 2$) as extracted from the dimer geometries (black (A) and gray (B) sticks). Values of the oscillator strength are reported in Table 1 and in the Supporting Information.

and the absorption measurements reported for the segregated (form I) and mixed inter-chain (form II) phases, respectively.

Given this qualitative resemblance, in order to provide a molecular based explanation for the main optical variations upon melt-annealing of the films, we performed DFT and TDDFT calculations on P(NDI2OD-T2) model systems consisting of molecular clusters made by two oligomers, each of them featuring two repeat units ($n = 2$), as reported in **Figure 2** (alkyl chains have been substituted with methyl groups). Inspired by the two polymorphs obtained by Brinkmann et al.,[46] we considered two distinct configurations, which we indicate with segregated and mixed (Figure 2). The structures were fully optimized taking into account intermolecular dispersion interactions at the ωB97XD/6–311G* level. Figure 2 reports the optimized structures of the two different dimers (generally indicated as $AB^{segregated}$ and AB^{mixed}), their computed TDDFT absorption spectra, and the vertical transitions for both the aggregates and the extracted isolated oligomers (A and B). **Table 1** collects details regarding the first low lying excited states in the systems considered. Due to the finite size of the dimers, calculations cannot be quantitative and the computed transition energies result to be higher than the measured ones; however, the spectral assignments can be accurately done based on the analysis of the character of the electronic transition involved.[45] Fundamental differences in the excited states between the two dimers can be evidenced. In the segregated dimer the two chromophores are highly interacting and strong intermolecular coupling amongst excited states occurs. As reported in Figure 2, the segregated dimer shows two low lying excited states, $S_1^{AB} = 2.50\,eV$ and $S_2^{AB} = 2.61\,eV$, having an oscillator strength f of 0.22 and 2.26, respectively, and differing in their nature and character from the first excited state of the two constituent molecules (S_1^A or S_1^B). Due to strong intermolecular exciton coupling,[47,48] S_1^{AB} and S_2^{AB} represent a new set of excited states, redshifted in energy and resulting from a linear combination[49–51] of the S_1^A and S_1^B excited state wavefunctions of the single chromophores.[49] While S_2^{AB} is prevalently localized on one oligomer (see Supporting Information, S4.2), thus recalling the properties of the single chain (see also the high oscillator strength and the polarization (x,y,z components) of the transition dipole moments reported in Table 1), S_1^{AB} is completely delocalized over the dimer structure, and its polarization acquires a higher projection than that of S_2^{AB} in the direction perpendicular (y) to the polymer chain (x). Following the analysis of the computed electronic transitions, we can associate S_1^{AB} to the low energy absorption band (the aggregate induced shoulder[45] observed in the experimental spectra around 1.55 eV), while S_2^{AB} corresponds to the band at 1.77 eV (see Figure 1).

On the other hand, in the mixed dimer configuration the excited states picture differs from the segregated one. The first two low lying dipole allowed excited states of the dimer are predicted as an independent superposition of the two oligomers. The energies of the two states, S_1^{AB} and S_2^{AB}, are indeed rather similar to S_1^B and S_1^A respectively, as indicated in Table 1. From the molecular orbital analysis (see Supporting Information, S4.2) and the transition dipole moment components, it turns out that in this molecular configuration the excited states of the dimer result to be more localized on the single oligomers rather than delocalized over the whole cluster.

Table 1. Evaluated parameters involved in the main optical transitions: TD-ωB97XD/6–31G* vertical transition energy (*E*), oscillator strength (*f*), molecular orbitals involved during the transition (MOs), transition dipole moment components (*x*,*y*,*z*) of the low lying excited states (as discussed in the text) for the segregated ($AB^{segregated}$) and mixed (AB^{mixed}) dimers and for the oligomers as extracted from the dimers.

	$AB^{segregated}$				AB^{mixed}			
	E (eV)	*f*	MOs	*x*/*y*/*z*	*E* (eV)	*f*	MOs	*x*/*y*/*z*
S_1^{AB}	2.50	0.22	H → L H → L+1 H–1 → L	1.81/0.55/0.03	2.59	0.84	H → L H → L+2	–3.59/–0.52/–0.07
S_2^{AB}	2.61	2.26	H → L H–1 → L+1 H → L+2	–5.85/–1.06/–0.00	2.80	1.28	H → L+1 H–1 → L+1	–4.15/–1.19/–0.21
	A from segregated				A from mixed			
	E (eV)	*f*	MOs	*x*/*y*/*z*	*E* (eV)	*f*	MOs	*x*/*y*/*z*
S_1^{A}	2.65	1.48	H → L	–4.67/1.00/–0.02	2.62	1.41	H → L	4.60/0.88/0.06
	B from segregated				B from mixed			
	E (eV)	*f*	MOs	*x*/*y*/*z*	*E* (eV)	*f*	MOs	*x*/*y*/*z*
S_1^{B}	2.70	1.5	H → L	–4.66/0.97/0.03	2.83	1.13	H → L	3.90/1.00/0.00

We have also computed the vertical excitation energies for a fully optimized, isolated oligomer of two repeating units ($n = 2$) of P(NDI2OD-T2), as reported in the Supporting Information, S4.8 and S4.11. Its equilibrium geometry is more distorted (in terms of dihedral angles between the NDI2OD and T2 units, see Supporting Information, S4.1) than that of the oligomers extracted from the dimers (see Supporting Information), in accordance with previous literature.[45] However, the redshift of the excited state energies of the segregated dimer cannot be explained only on the basis of a packing-induced planarization of the molecules in the dimer (see ref. [45]), and intermolecular excitonic effects[49] have to be considered to fully assign and describe the spectral differences upon aggregation.

To further support our conclusions we computed, at the TDDFT level, the excited states of a large supramolecular cluster featuring four stacked chains of $n = 2$ oligomers of P(NDI2OD-T2), both arranged in the segregated and the mixed pattern. Results, reported in the Supporting Information S4.3, confirm the presence of delocalized, low-energy excited states all over the cluster for the segregated configuration rather than the mixed one, thus validating the assignment of the low energy band (1.55 eV) of the P(NDI2OD-T2) absorption spectra.

To summarize this section, we have shown that the low energy optical transition (shoulder) at 1.55 eV, which is related to an intermolecular, delocalized excited state highly sensitive to the local aggregate geometry, is a spectral signature to monitor the structural properties and local packing of the polymeric film at the molecular level.

Overall, we conclude that the melt-annealing process, besides re-orienting the crystalline domains within the film and the polymer chains as observed by Rivnay et al.[41] and by Giussani et al.,[52] respectively, induces a rearrangement of the local packing of the conjugated segments.

2.2. Electrical Characterization

In order to electrically characterize transport properties in both pristine and melt-annealed P(NDI2OD-T2) films, we fabricated top-gate OFETs. In these devices, electrons are accumulated at the semiconductor-dielectric interface when a positive potential is applied to the gate electrode. The transfer and output characteristics, reported in **Figure 3**, monitor the modulation of the source-drain current (I_{ds}) upon gate voltage (V_g) variation at a constant source drain voltage (V_{ds}), and its modulation when V_g is kept constant and V_{ds} is modulated. A reduction of the overall channel current at the same bias point can be observed for the melt-annealed P(NDI2OD-T2) based OFET compared to the pristine film. While this effect might suggest a reduction of the charge mobility, it is instead only due to a variation of the injection properties upon melt-annealing. Qualitatively, this claim is supported by two observations: a) melt-annealing induces an increase in the threshold voltage of the device, as shown in Figure 3a; b) the output curves in Figure 3b show a marked S-shape for the melt-annealed sample at low V_d.[53] In accordance with these results, it was previously reported that melt-annealing produces a reduction of the vertical bulk conductivity in P(NDI2OD-T2),[41] which directly contributes to increase the resistance of the bulk access to the OFET channel.[53]

Apparent mobilities, those extracted without taking into account contact resistance effects, are very similar for both films in the linear regime (0.053 and 0.030 $cm^2\ V^{-1}\ s^{-1}$ for pristine and melt-annealed films, respectively), suggesting limited contact resistance values. Indeed, owing to the high lateral field promoting injection, apparent saturation mobilities are exactly the same (0.14 $cm^2\ V^{-1}\ s^{-1}$). We further quantified the contact resistance R_C in the linear regime with the differential method[54] to assess its variation upon melt-annealing; data are reported in Table 1. R_C is 17 kΩ cm for the pristine film and it

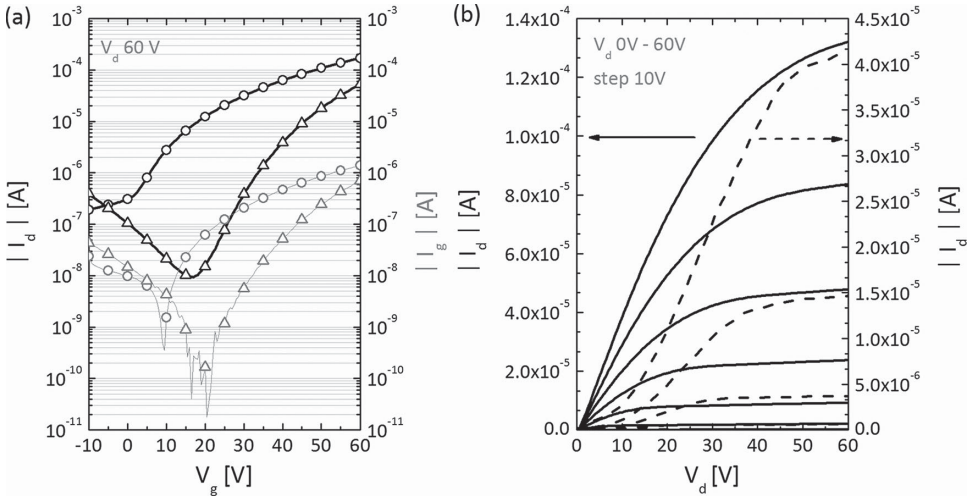

Figure 3. a) Transfer characteristic curves of pristine (circles) and melt-annealed (triangles) P(NDI2OD-T2) FETs and b) output characteristic curves of pristine (continuous lines) and melt-annealed (dashed lines) P(NDI2OD-T2) FETs; in (a) the black thick lines represent the drain current in the saturation regime (V_d = 60 V) and the thin gray lines represent the gate leakage current in the saturation regime; curves in (b) have been taken at V_g values ranging from 0 to 60 V with steps of 10 V.

increases to 40 kΩ cm for the melt-annealed one, confirming the picture described above. Consequently, calculated intrinsic linear mobilities show only a slight variation compared to apparent values.

As suggested in a recent work by Schuettfort et al.,[42] a first explanation for the reported evidences is that melt-annealing only modifies the bulk of the film and therefore the injection, and not the surface where the channel is actually formed in the case of a top-gate OFET. However, in this work they characterized the relative orientation of the polymer backbone but not the local packing of the polymer segments. Alternatively, if the local packing modification affected the bulk and the surface of the material in the same way, we would be left with the conclusion that the specific structural modification induced by thermal treatment cannot affect the carrier mobility.

To elucidate this aspect we have performed CMS measurements on working OFETs to directly access only those polymer segments probed by the mobile charges at the semiconductor-dielectric interface.

2.3. Charge Modulation Spectroscopy

CMS measures the variation of the polymer optical absorption induced by charge accumulation. A positive CMS signal indicates an increase of the transmitted light ($\Delta T > 0$) and is associated with the bleaching of the absorption of neutral polymer segments due to the presence of charges on the backbone, while a negative CMS signal indicates a reduction of transmitted light ($\Delta T < 0$) due to charge-induced absorption. CMS intrinsically provides only spectral features of conjugated segments actually probed by charges. Because the charge transport channel in a field effect transistor, which is the device investigated by CMS, is limited to a few molecular layers below the dielectric, CMS selectively probes only the charge induced features at the interface between the polymer semiconductor and the dielectric and not the entire polymer film bulk. Moreover, since it is a modulated spectroscopy technique, CMS can only record spectral features induced by mobile carriers, the ones actually contributing to charge transport, and not by deeply trapped, immobile ones. In **Figure 4** the CMS spectra collected on a pristine P(NDI2OD-T2) based OFET at different temperatures are reported. According to previous work,[55,56] close to room temperature (290 K) we observe a broad central bleaching band that recalls the UV-Vis absorption spectrum and charge-induced absorption at lower energies. Three main bleaching features are evident at 1.55, 1.77, and 1.90 eV, corresponding, as discussed before, to the assigned intermolecular excited state, the intramolecular CT, and its vibronic replica, respectively. The main charge-induced absorption feature peak appears at 1.45 eV.

The partial overlap of the bleaching and charge-induced absorption signals at room temperature precludes the

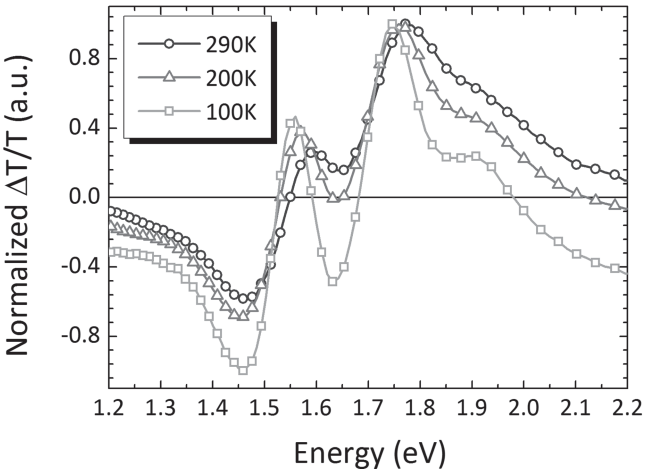

Figure 4. CMS spectra of a pristine, P(NDI2OD-T2) based OFET at 290, 200, and 100 K normalized to the central bleaching peak at 1.77 eV. The measurements were taken with an applied 60 V bias on the gate electrode, modulated with a 25 V AC signal.

possibility to clearly resolve the two signals. In order to have a better spectral resolution we performed the same CMS measurements at lower temperatures (Figure 4). As expected, by decreasing the temperature the broadening of each spectral feature is reduced. The spectrum collected at 100 K reports better resolved bleaching spectral features showing a spectral redshift of ≈0.025 eV with respect to the spectrum at 290 K. For both the low energy bleaching peaks at around 1.55 and 1.77 eV, the spectral shift is assigned to the reducing overlap between these bleaching transitions and the underlying charge induced absorption transition.

The most interesting aspect in the low temperature (100 K) CMS spectra is the appearance of an absorption band ($\Delta T/T < 0$) peaking at 1.63 eV, indicating that the deep at 1.65 eV observed in the spectrum close to room temperature (290 K) is actually due to an absorption feature, distinct from the one observed at 1.45 eV. We have therefore evidenced a complex spectral charge-induced pattern for P(NDI2OD-T2) pristine films, where the charge-induced absorption is composed of at least two distinct bands peaking at 1.45 and 1.63 eV, respectively. One crucial aspect is to clarify whether these transitions are associated with the same charged polymer segment (*intra*-molecular polaron) or with two distinctive polarons with a different degree of delocalization.[23,57]

To this extent, CMS measurements on the melt-annealed P(NDI2OD-T2) based OFET, performed to investigate the effects of the structural modifications on the charged-induced signals, provide us with compelling evidences. In **Figure 5** the CMS spectra collected at room temperature (approximately 295 K) on both the pristine and melt-annealed P(NDI2OD-T2) films are reported together with the absorption spectra. The bleaching signals of the two CMS spectra peak at 1.77 and 1.90 eV, in agreement with the UV-Vis spectra (reported in solid lines). We do observe modifications of the CMS spectrum of the melt-annealed film with respect to the pristine film. As far as the bleaching features are concerned, these modifications resemble the modifications observed in the UV-Vis absorption measurement, which probes the entire bulk films: there is a relative increase of the vibronic replica at 1.90 eV and a decrease of the low-energy shoulder around 1.55 eV assigned before to an intermolecular excited state (Figure 2). This observation holds an important implication: charges probe conjugated segments that undergo the same local structural rearrangement upon thermal annealing as observed in the bulk. Since the carrier mobility is not substantially affected, as demonstrated in the previous section, we conclude that the local molecular packing cannot represent the bottleneck for charge transport over the 40 μm channel length of the devices under test and this has to be looked for on a different length scale.[22]

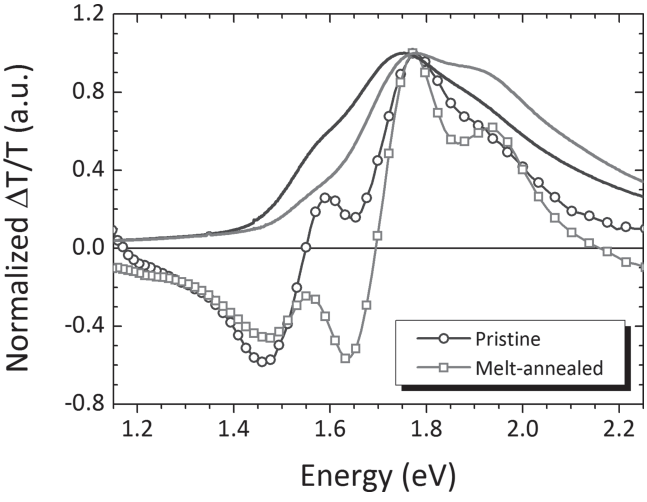

Figure 5. CMS spectra of pristine and melt-annealed P(NDI2OD-T2) based OFETs at room temperature (295 K). The measurements were taken by biasing the gate electrode at 80 V and by superimposing a 10 V AC voltage (amplitude). The solid lines present the absorption spectra already shown in Figure 1; each curve is normalized to its maximum ($\Delta T/T \approx 6 \times 10^{-4}$ for the pristine based OFET and $\Delta T/T \approx 7 \times 10^{-4}$ for the melt-annealed based OFET).

The melt-annealed P(NDI2OD-T2) film also shows the two distinct charge absorption transitions observed only at 100 K in the pristine film, arising at 1.45 and 1.63 eV; however, they are already well resolved at room temperature (Figure S3, Supporting Information) as a consequence of the reduced intensity of the overlapping bleaching band at 1.55 eV. Therefore, in both cases we observe charge-induced transitions originating from the same polaronic species with no appearance of additional charge-induced bands. Since a different spatial extension of the polaronic species in the two cases would imply transitions at different energies,[58] we infer that the structural modifications induced by melt-annealing do not modify the polaron extension, i.e., the electronic states that constitute the bottleneck for charge transport are unaffected. In particular, it is worth highlighting that the latter is true although the charge is bleaching either aggregated or isolated polymeric segments (i.e., pristine vs. melt-annealed films).

Moreover, from the analysis of the UV-Vis absorption spectra, we observed that going from the pristine to the melt-annealed film, the intermolecular optical transition at 1.55 eV is reduced. If the charges in the pristine film were as well characterized by a delocalization over adjacent polymer chains (i.e., an interchain polaron), one could expect that by changing the local packing motif of the conjugated chains, some transitions would change their energy or become allowed due to different intermolecular interactions, like in the model proposed for polythiophene derivatives where interchain interactions cause a splitting of the charge-induced absorption band, as observed in previous CMS investigations.[19,23] However, we do not observe any energy shift or splitting of the charge-induced transitions (Figure 5), which strongly suggests a mainly intramolecular character of the polaron.

It is to be noted that the intensity ratio between the two absorption features (at 1.45 and 1.63 eV) varies: while this can be partially due to a reduction of the overlap of the absorption with the low energy bleaching feature upon melt-annealing, a redistribution of the oscillator strength between the two transitions subsequent to the annealing treatment can also contribute. In a scenario where the two transitions can be assigned to the same carrier species localized on a single conjugated segment, the oscillator strength redistribution should be the result of a local effect as a consequence of a varied electronic density (i.e., polarizability) surrounding each conjugated segment.

To better elucidate the nature of the polaronic species, DFT and TDDFT calculations were performed, also on charged oligomer chains of P(NDI2OD-T2), and compared to the experimental results.

2.4. DFT and TDDFT Calculations on a Charged P(NDI2OD-T2) Chain

We have recently shown[44] that range separated DFT functionals, such as CAM-B3LYP, can predict a finite value for the intramolecular reorganization energies (λ_i^e and λ_i^h) of P(NDI2OD-T2) at the polymer limit ($n \rightarrow \infty$), thus reasonably describing[55] the polaron formation. The structural relaxation of the additional electron (hole) on the isolated oligomer results to be confined over a finite segment length[44,55] that, at the CAM-B3LYP/6–31G* level (similar results obtained with the ωB97XD functional), involves three/four repeat units (n = 3,4) of P(NDI2OD-T2). This result implies that, while at least seven repeat units (n = 7) are necessary to correctly describe the electronic/optical properties of the neutral polymer species, as shown in ref. [44,55], three/four units are enough for the charged species because the polaron is strongly localized, thus being not too much affected by longer chain lengths.

To properly describe the electronic structure and transitions of the charged species we therefore chose to study single chain oligomers featuring four and five repeat units (n = 4,5), which can be considered as good models for the charged polymer chain, giving also the possibility to test the effects of two different chain lengths onto the electronic properties of the charged species (see Supporting Information, S4.4, S4.5, and S4.12–S4.15).

The TDDFT computed electronic transitions for the negatively charged n = 4 oligomer, together with the spectrum shape (black solid line), are reported in **Figure 6** (1.2–2.2 eV energy region). The energy values reported in Figure 6 for the vertical transitions are scaled values, where the scaling factor used is 0.78 in order to match the experimental results (unscaled values are reported in the Supporting Information, S4.4 and S.14–S4.15).

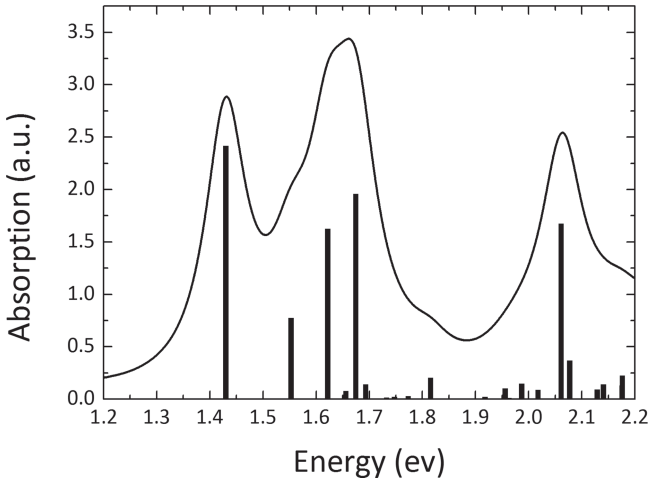

Figure 6. TDDFT (UCAM-B3LYP)/6–31G* computed electronic transitions for a P(NDI2OD-T2) oligomer with n = 4, in the charged (–1) electronic singlet state. Electronic spectrum obtained by a convolution with Lorentzian functions with a full width at half maximum FWHM = 0.05 eV. Values of the oscillator strength are reported in the main text and in the Supporting Information.

In the reported spectral region there are four main transitions: i) 1.42 eV with oscillator strength f = 0.48, ii) 1.55 eV, f = 0.15, iii) 1.61 eV, f = 0.32, and iv) 1.66 eV, f = 0.39. The single-occupied and unoccupied molecular orbitals involved in each transition, as reported in the Supporting Information S4.5, mainly involve localized excitations from the single NDI2OD unit to the T2 group as well as to the whole NDI2OD-T2 unit. Another intense transition is computed at high energy, 2.05 eV, f = 0.33, involving localized molecular orbitals on either the donor or the acceptor unit. This band is not clearly visible in the CMS spectrum because of the overlap with the strong bleaching band; however, an absorption band starting at 2.1 eV is observable in the CMS spectra of the 100 K pristine (Figure 4) and melt-annealed film (Figure 5).

The computed electronic spectrum of the n = 4 P(NDI2OD-T2) charged species (Figure 6) well reproduce CMS spectra of both pristine and melt-annealed films in the 1.3–1.7 eV region (Figure 5), dominated by two main absorption features. We therefore infer that the CMS band at 1.45 eV can be assigned to the calculated electronic transition i) centred at 1.42 eV, while the CMS band at 1.63 eV is the result of a convolution of at least two close transitions iii)–iv) at 1.61 eV and 1.66 eV, respectively.

To rule out any effects induced by the chain length to the electronic transitions, we have also considered the case of n = 5 P(NDI2OD-T2) (see Supporting Information, S4.4, S4.13, S4.15). The dipole active electronic transitions of the charged n = 5 oligomer show little difference with respect to n = 4 (≈0.04 eV shift), thus confirming that the polaron is localized, being not so much affected by the chain length, and at the same time implying that n = 4 turns out to be a good model system for describing the electronic properties of P(NDI2OD-T2) polaronic species.

According to our experimental and computational evidences, we can conclude that the bands observed in the CMS spectra (both pristine and melt-annealed films) are due to polarons localized on a single P(NDI2OD-T2) chain (i.e., intrachain polaron), confined onto three to four repeat units (see also [44]).

We further notice that the computed spectral shape and the intensity ratio of the peaks at 1.45 and 1.63 eV (Figure 6) are much more similar to the CMS spectrum of the melt-annealed films (squares in Figure 5). This is not surprising if we recall that the CMS spectrum of the melt-annealed film is the one which more strongly resembles the single chain case, as revealed by the analysis of the UV-Vis absorption spectra (Figure 1,2). Therefore, as hypothesized in the previous section, the difference in the relative ratio of the charge-induced absorption transitions for the pristine case must originate from the different electronic density surrounding the charged moiety. From the bleaching signal in pristine films we know that charges probe molecular aggregates but, irrespective of this, they show similar polaronic relaxations as the melt-annealed samples, being confined within 3–4 monomers of a single polymer chain.

3. Conclusions

The nature of charge carriers in P(NDI2OD-T2), a good electron transporting polymer exemplary of a more wide and general class of naphtalenediimide based donor-acceptor materials,[59–62] has been investigated via a broad set of experiments, encompassing UV-Vis, CMS spectroscopy, and DFT calculations. The charge-induced bleaching signal probed in the channel of a field-effect device first demonstrates that the rearrangement of molecular packing, which follows a melt-annealing process of the film, is effective not only in the bulk but also at the semiconductor-dielectric interface, where the charge accumulates. The structural rearrangements are monitored by variations of the UV-Vis absorption spectra. In particular the band centred at 1.55 eV, assigned to an intermolecular exciton, is extremely sensitive to the local polymer packing, and its intensity decreases going from pristine to melt-annealed films. Based on DFT and TDDFT calculations on model dimer systems we found an activation of this band for segregated structures and a quenching for mixed ones. This observation follows what was previously observed for two different, ad hoc prepared, ordered, epitaxially grown polymorphs of P(NDI2OD-T2),[46] characterized by a segregated and mixed stacking of NDI2OD and T2 units, which can qualitatively be associated with the prevalent packing in the pristine and in the melt-annealed film, respectively.

We have verified that upon melt-annealing of P(NDI2OD-T2) films, only charge injection is modified in top-gate field-effect devices, while charge transport, i.e., the carrier mobility, remains almost unaffected. In accordance with this observation, CMS data, recorded on the same devices, reveal polaronic absorption features in the low energy spectral region (1.2–1.7 eV), featuring the same energy transitions in both pristine and melt-annealed films with a different intensity ratio of the two active bands (1.45 and 1.63 eV). The presence of polaron transitions at the same energy in both films is a strong experimental evidence that the relaxed states probed by mobile charges are of the same nature (i.e., spatial extension), irrespective of the profound structural modifications. TDDFT calculations on isolated polymer segments very nicely reproduce the main absorptions of charged species between 1.2 and 1.7 eV. This result indicates that charges in P(NDI2OD-T2) are localized on single chains and have therefore an intrinsic intramolecular character.

The above combined experimental and theoretical results are consistent: indeed, if the polaron was delocalized over adjacent segments, modifications in the charge-induced absorption features and in the overall charge mobility would be expected to occur as a result of profound differences in the local packing induced by the thermal treatment.[41,52]

We can compare these findings with the work by Luzio et al.[22] who reported a clear effect of macro-scale ordering in P(NDI2OD-T2) on the charge carrier mobility. In that case, an increase of the field-effect mobility was achieved by improving the reciprocal orientation of solvent-induced supra-molecular fibrillar structures over tens of microns, a scale-length comparable to the channel length of devices. Interestingly, this mobility change was not associated with a modification of the local molecular packing, as probed by UV-Vis and CMS measurements, therefore representing a complementary example to the one described here, where instead no substantial variation of mobility is recorded upon modification of the nanoscale molecular structure.

We therefore conclude that overall charge transport in P(NDI2OD-T2) can be described as a hopping process of a highly localized, intrachain polaron. The delocalization of interchain polarons is not strictly necessary to observe field-effect mobility values in the 0.1–1 $cm^2\ V^{-1}\ s^{-1}$ range in semiconducting polymer films. To explain this relatively high mobility value, we can speculate that intrachain transport is favoured by low energetic barriers due to efficient intrachain coupling, so that interchain hopping can occur only at more energetically favoured interhopping sites. Indeed, strong electronic coupling can develop between conjugated segments of P(NDI2OD-T2) chains, as recently reported.[44,63] In this scenario, high interconnectivity[64] and long range orientational order,[22] which characterize the film microstructure, allow for many hopping sites and become crucial parameters in sizing the field-effect mobility along tens of microns long channels in OFET devices.

4. Experimental Section

Sample Preparation: Thoroughly cleaned 1737F glass was used as substrates for all the films investigated in this work. FETs were fabricated according to a top-gate, bottom-contact architecture. Bottom Au contacts were defined by a lift-off photolithographic process with a 0.7 nm thick Cr adhesion layer. The thickness of the Au contacts was 30 nm. Patterned substrates were cleaned in an ultrasonic bath in isopropyl alcohol for 2–3 min before deposition of the semiconductor. P(NDI2OD-T2) was purchased from Polyera Corporation (Activink N2200). A solution of P(NDI2OD-T2) in 1,2-dichlorobenzene (9 g l^{-1}) was prepared, filtered, and deposited by spin-coating at 1000 rpm for 90 s in a nitrogen glove box. The semiconductor was then annealed for 14 h at 120 °C on a hot plate in a nitrogen atmosphere in the case of devices based on pristine films, and annealed for 40 min at 350 °C (cooling rate 10 °C/min) on a hot plate in a nitrogen atmosphere in the case of devices based on melt-annealed films. Values for the linear and saturation mobility, threshold voltage, and contact resistance reported in **Table 2** were extracted from OFETs using polymethyl methacrylate (PMMA) as the dielectric layer. PMMA (Sigma-Aldrich) with M_w = 120 kg mol^{-1} was spun from 2-butanone (MEK) (with a concentration of 70 g l^{-1}). A dielectric layer thickness of 660 nm was obtained. After deposition of the dielectric, the devices were annealed under nitrogen on a hot-plate at 80 °C for 4 h. 30 nm thick gate Al electrodes were thermally evaporated as gate contacts.

Table 2. OFET operating parameters: mobility (μ) and threshold voltage (V_t) both in the linear (subscript "lin") and saturation ("sat") regime, and contact resistance R_C extracted in the linear regime for both pristine and melt-annealed P(NDI2OD-T2) based OFETs. In the linear regime, where R_C can be quantified, both apparent ("app") and intrinsic mobility values ("intr") are reported.

Thermal treatment	$\mu_{lin\ app}$ [$cm^2\ V^{-1}\ s^{-1}$]	$\mu_{lin\ intr}$ [$cm^2\ V^{-1}\ s^{-1}$]	μ_{sat} [$cm^2\ V^{-1}\ s^{-1}$]	$V_{t,\ sat}$ [V]	$V_{t,\ lin}$ [V]	R_C [kΩ cm]
Pristine	0.053 ± 0.012	0.056 ± 0.001	0.14 ± 0.014	15 ± 2	5 ± 1	≈17 ± 3
Melt-annealed	0.030 ± 0.004	0.041 ± 0.002	0.14 ± 0.010	24 ± 3	17 ± 3	≈40 ± 6

For samples studied by CMS, polystyrene (PS, Sigma-Aldrich) with M_w = 290 kg mol^{-1} was spun from 2-butanone (MEK) (50 g l^{-1}). A dielectric layer thickness of 500 nm was obtained. After deposition of the dielectric the devices were annealed under nitrogen on a hot-plate at 80 °C for 4 h. Thermally evaporated 4.5 nm thick Au semi-transparent gate electrodes were employed.

Electrical Characterization: Electrical characteristics of the transistors were measured in a nitrogen glovebox on a Wentworth Laboratories probe station with an Agilent B1500A semiconductor parameter analyser. Linear charge carrier mobility values were extracted from the transfer characteristic curves according to the gradual channel approximation,[65] following the expression $I_d = \mu_{lin} C_{die} W L^{-1} [(V_g - V_t)V_d - V_d^2/2]$, where I_d is the drain current, μ_{lin} is the linear mobility, C_{die} is the specific dielectric capacitance, W and L are the width and the length of the channel, respectively, V_g is the gate voltage, V_d is the drain voltage, and V_t is the threshold voltage. Saturation charge carrier mobility values were extracted from the transfer characteristic curves according to the expression $I_d = \mu_{sat} C_{die} W (2L)^{-1} (V_g - V_t)^2$, where μ_{sat} is the saturation mobility. Accordingly, the V_g dependent values of μ_{lin} (μ_{sat}) were obtained from the slope of I_d vs. V_g ($I_d^{1/2}$ vs. V_g), calculated every three points around each V_g value. V_t values were extracted in both regimes with the second derivative method.[66]

UV-Vis Absorption: Absorption measurements were performed using a Perkin Elmer Lambda 1050 spectrometer. The samples for the absorption measurements were prepared by spin-coating the material on quartz substrates and subsequent annealing according to the same protocol used for OFET preparation described above in the sample preparation section.

Charge Modulation Spectroscopy: CMS spectra were collected by measuring the normalized transmittance variation ($\Delta T/T$) induced by applying a modulated voltage. We performed the measurements by keeping the source and drain electrode at 0 V, while the modulated voltage (f = 1127 Hz) was applied at the gate electrode. The offset voltage and amplitude of modulation varied from sample to sample. Details on these values may be found in the figure captions.

The probing light was obtained by monochromating a tungsten lamp source. Once monochromated the light was focused on the device and then the transmitted light was collected and revealed using a silicon photodiode. The electrical signal was amplified through a trans-impedance amplifier (Femto DHPCA-100) and then revealed using a DSP Lock-in amplifier (Standford Instrument SR830).

All the measurements were performed in a continuous flow static exchange gas cryostat (Oxford instrument). The cryostat consisted of three chambers, one inside the other. The sample was placed inside the internal chamber filled with gaseous He. Cryogenic liquid (He) was then fluxed inside the second chamber allowing temperature control of the He atmosphere inside the sample chamber. Eventually, a third chamber was evacuated (≈10^{-5}–10^{-6} mbar) in order to assure thermal isolation from the external ambient.

DFT and TDDFT Calculations: Dimers of P(NDI2OD-T2) consist of two oligomers (chain length n = 2) facing each other in two different configurations, namely segregated and mixed. Dimers were fully optimized using the range separated functional ωB97XD[67] with the inclusion of dispersion forces, and the triple split 6–311G** basis set with inclusion of polarization functions. A conductor polarisable continuum model (CPCM)[68] has been applied to mimic the effect of the medium using the dielectric constant of the toluene solvent.[45] TDDFT vertical excitation energies were computed, using the 6–31G* basis set, on the optimized geometries by considering more than 50 excited states for each dimer. The same TDDFT calculations were applied for the oligomers (two for each dimer) extracted from the aggregate optimized geometry. For comparison, a single oligomer n = 2 was fully optimized at the same level of theory (ωB97XD/6–311G*) to discriminate the structural effects induced by aggregation.

Bigger clusters than the dimers were considered. Two four-stuck oligomer (n = 2) clusters were generated by replicating the two dimer aggregates, and TDDFT calculations (ωB97XD/6–31G*) have been performed for these not optimized geometries (see Supporting Information, S4.3, for a comparison between the computed spectra as obtained from the dimers and the four-stuck oligomers).

Charged species were studied at the unrestricted UCAM-B3LYP/6–31G* level; however, similar results have been obtained using ωUB97XD. The geometry of oligomers featuring four and five, n = 4, 5, repeat units have been fully optimized in their stable minimum. TDDFT (UCAMB3LYP/6–31G*) vertical electronic transitions on the optimized charged species were computed considering 50 excited states for n = 4 and 20 excited states for n = 5. A comparison was reported in the Supporting Information, S4.4, S4.5, and S4.12–S4.15. All calculations were performed using the Gaussian09 program.[69]

Supporting Information

Supporting Information is available from the Wiley Online Library or from the author.

Acknowledgements

The authors thank Francesco Maddalena, Giuseppina Pace, and Nicola Martino for support in different stages of the work and for helpful discussions. Financial support is acknowledged from Fondazione Cariplo under project Indixi, Grant No. 2011–0368, and from the European Union through the Marie-Curie Career Integration Grant 2011"IPPIA", within the EU Seventh Framework Programme (FP7/2007–2013) under grant agreement No. PCIG09-GA-2011–291844.

Received: February 5, 2014
Revised: April 13, 2014
Published online: July 10, 2014

[1] H. Sirringhaus, T. Sakanoue, J.-F. Chang, *Phys. Status Solidi B* **2012**, *249*, 1655.
[2] N. Zhao, Y.-Y. Noh, J.-F. Chang, M. Heeney, I. McCulloch, H. Sirringhaus, *Adv. Mater.* **2009**, *21*, 3759.
[3] A. Troisi, *Chem. Soc. Rev.* **2011**, *40*, 2347.
[4] R. Ponce Ortiz, H. Herrera, M. J. Mancheño, C. Seoane, J. L. Segura, P. Mayorga Burrezo, J. Casado, J. T. López Navarrete, A. Facchetti, T. J. Marks, *Chemistry* **2013**, *19*, 12458.
[5] A. C. Arias, J. D. MacKenzie, I. McCulloch, J. Rivnay, A. Salleo, *Chem. Rev.* **2010**, *110*, 3.
[6] C. J. Brabec, S. Gowrisanker, J. J. M. Halls, D. Laird, S. Jia, S. P. Williams, *Adv. Mater.* **2010**, *22*, 3839.
[7] K.-J. Baeg, M. Caironi, Y.-Y. Noh, *Adv. Mater.* **2013**, *25*, 4210.
[8] K. Sen, R. Crespo-Otero, O. Weingart, W. Thiel, M. Barbatti, *J. Chem. Theory Comput.* **2013**, *9*, 533.
[9] H. Usta, A. Facchetti, T. J. Marks, *Acc. Chem. Res.* **2011**, *44*, 501.
[10] A. Facchetti, *Chem. Mater.* **2011**, *23*, 733.
[11] X. Zhan, A. Facchetti, S. Barlow, T. J. Marks, M. a Ratner, M. R. Wasielewski, S. R. Marder, *Adv. Mater.* **2011**, *23*, 268.
[12] H. Klauk, *Chem. Soc. Rev.* **2010**, *39*, 2643.
[13] W. Smaal, C. Kjellander, Y. Jeong, A. Tripathi, B. Van Der Putten, A. Facchetti, H. Yan, J. Quinn, J. Anthony, K. Myny, W. Dehaene, G. Gelinck, *Org. Electron.* **2012**, *13*, 1686.
[14] G. Gelinck, P. Heremans, K. Nomoto, T. D. Anthopoulos, *Adv. Mater.* **2010**, *22*, 3778.
[15] V. Podzorov, E. Menard, J. Rogers, M. Gershenson, *Phys. Rev. Lett.* **2005**, *95*, 226601.
[16] Y. Okada, K. Sakai, T. Uemura, Y. Nakazawa, J. Takeya, *Phys. Rev. B* **2011**, *84*, 245308.
[17] J.-F. Chang, T. Sakanoue, Y. Olivier, T. Uemura, M.-B. Dufourg-Madec, S. G. Yeates, J. Cornil, J. Takeya, A. Troisi, H. Sirringhaus, *Phys. Rev. Lett.* **2011**, *107*, 066601.

[18] A. S. Eggeman, S. Illig, A. Troisi, H. Sirringhaus, P. a Midgley, *Nat. Mater.* **2013**, *12*, 1045.
[19] Z. Chen, M. Bird, V. Lemaur, G. Radtke, J. Cornil, M. Heeney, I. McCulloch, H. Sirringhaus, *Phys. Rev. B* **2011**, *84*, 1.
[20] J.-L. Brédas, D. Beljonne, V. Coropceanu, J. Cornil, *Chem. Rev.* **2004**, *104*, 4971.
[21] N. Tessler, Y. Preezant, N. Rappaport, Y. Roichman, *Adv. Mater.* **2009**, *21*, 2741.
[22] A. Luzio, L. Criante, V. D'Innocenzo, M. Caironi, *Sci. Rep.* **2013**, *3*, 3425.
[23] H. Sirringhaus, P. J. Brown, R. H. Friend, M. M. Nielsen, K. Bechgaard, B. M. W. Langeveld-Voss, A. J. H. Spiering, R. A. J. Janssen, E. W. Meijer, P. Herwig, D. M. de Leeuw, *Nature* **1999**, *401*, 685.
[24] J. Northrup, *Phys. Rev. B* **2007**, *76*, 245202.
[25] D. M. DeLongchamp, R. J. Kline, E. K. Lin, D. A. Fischer, L. J. Richter, L. A. Lucas, M. Heeney, I. McCulloch, J. E. Northrup, *Adv. Mater.* **2007**, *19*, 833.
[26] R. W. I. de Boer, M. E. Gershenson, A. F. Morpurgo, V. Podzorov, *Phys. Status Solidi A* **2004**, *201*, 1302.
[27] A. Salleo, T. W. Chen, a. R. Völkel, R. A. Street, *Phys. Rev. B* **2004**, *70*, 115311.
[28] S. Mehraeen, V. Coropceanu, J.-L. Brédas, *Phys. Rev. B* **2013**, *87*, 195209.
[29] A. Salleo, *Mater. Today* **2007**, *10*, 38.
[30] S. Ciuchi, S. Fratini, *Phys. Rev. Lett.* **2011**, *106*, 166403.
[31] Z. Chen, M. J. Lee, R. Shahid Ashraf, Y. Gu, S. Albert-Seifried, M. Meedom Nielsen, B. Schroeder, T. D. Anthopoulos, M. Heeney, I. McCulloch, H. Sirringhaus, *Adv. Mater.* **2012**, *24*, 647.
[32] C. Hermosa, J. Vicente Álvarez, M.-R. Azani, C. J. Gómez-García, M. Fritz, J. M. Soler, J. Gómez-Herrero, C. Gómez-Navarro, F. Zamora, *Nat. Commun.* **2013**, *4*, 1709.
[33] T. Liu, A. Troisi, *Adv. Funct. Mater.* **2014**, *24*, 925.
[34] R. Noriega, J. Rivnay, K. Vandewal, F. P. V Koch, N. Stingelin, P. Smith, M. F. Toney, A. Salleo, *Nat. Mater.* **2013**, *12*, 1038.
[35] B.-G. Kim, E. J. Jeong, J. W. Chung, S. Seo, B. Koo, J. Kim, *Nat. Mater.* **2013**, *12*, 659.
[36] X. Zhang, H. Bronstein, A. J. Kronemeijer, J. Smith, Y. Kim, R. J. Kline, L. J. Richter, T. D. Anthopoulos, H. Sirringhaus, K. Song, M. Heeney, W. Zhang, I. McCulloch, D. M. DeLongchamp, *Nat. Commun.* **2013**, *4*, 2238.
[37] Z. Shuai, H. Geng, W. Xu, Y. Liao, J.-M. André, *Chem. Soc. Rev.* **2014**.
[38] H. Yan, Z. Chen, Y. Zheng, C. Newman, J. R. Quinn, F. Dötz, M. Kastler, A. Facchetti, *Nature* **2009**, *457*, 679.
[39] H. Xu, Y. Jiang, J. Li, B. S. Ong, Z. Shuai, J. Xu, N. Zhao, *J. Phys. Chem. C* **2013**, *117*, 6835.
[40] J. Rivnay, M. F. Toney, Y. Zheng, I. V Kauvar, Z. Chen, V. Wagner, A. Facchetti, A. Salleo, *Adv. Mater.* **2010**, *22*, 4359.
[41] J. Rivnay, R. Steyrleuthner, L. H. Jimison, A. Casadei, Z. Chen, M. F. Toney, A. Facchetti, D. Neher, A. Salleo, *Macromolecules* **2011**, *44*, 5246.
[42] T. Schuettfort, L. Thomsen, C. R. McNeill, *J. Am. Chem. Soc.* **2013**, *135*, 1092.
[43] T. Schuettfort, S. Huettner, S. Lilliu, J. E. Macdonald, L. Thomsen, C. R. McNeill, *Macromolecules* **2011**, *44*, 1530.
[44] D. Fazzi, M. Caironi, C. Castiglioni, *J. Am. Chem. Soc.* **2011**, *133*, 19056.
[45] R. Steyrleuthner, M. Schubert, I. Howard, B. Klaumünzer, K. Schilling, Z. Chen, P. Saalfrank, F. Laquai, A. Facchetti, D. Neher, *J. Am. Chem. Soc.* **2012**, *134*, 18303.
[46] M. Brinkmann, E. Gonthier, S. Bogen, K. Tremel, S. Ludwigs, M. Hufnagel, M. Sommer, *ACS Nano* **2012**, *6*, 10319.
[47] I. Hwang, G. D. Scholes, *Chem. Mater.* **2011**, *23*, 610.
[48] E. Collini, *Chem. Soc. Rev.* **2013**, *42*, 4932.
[49] M. Pope, C. E. Swenberg, *Electronic Processes in Organic Crystals and Polymers*, 2nd ed., Oxford University Press, Oxford, **1999**.
[50] F. C. Spano, S. C. J. Meskers, E. Hennebicq, D. Beljonne, *J. Am. Chem. Soc.* **2007**, *129*, 7044.
[51] F. C. Spano, *Annu. Rev. Phys. Chem.* **2006**, *57*, 217.
[52] E. Giussani, D. Fazzi, L. Brambilla, M. Caironi, C. Castiglioni, *Macromolecules* **2013**, *46*, 2658.
[53] D. Natali, M. Caironi, *Adv. Mater.* **2012**, *24*, 1357.
[54] D. Natali, L. Fumagalli, M. Sampietro, *J. Appl. Phys.* **2007**, *101*, 014501.
[55] M. Caironi, M. Bird, D. Fazzi, Z. Chen, R. Di Pietro, C. Newman, A. Facchetti, H. Sirringhaus, *Adv. Funct. Mater.* **2011**, *21*, 3371.
[56] C. Sciascia, N. Martino, T. Schuettfort, B. Watts, G. Grancini, M. R. Antognazza, M. Zavelani-Rossi, C. R. McNeill, M. Caironi, *Adv. Mater.* **2011**, *23*, 5086.
[57] M. J. Lee, D. Gupta, N. Zhao, M. Heeney, I. McCulloch, H. Sirringhaus, *Adv. Funct. Mater.* **2011**, *21*, 932.
[58] D. Beljonne, J. Cornil, H. Sirringhaus, P. J. Brown, M. Shkunov, R. H. Friend, J.-L. Brédas, *Adv. Funct. Mater.* **2001**, *11*, 229.
[59] M. Sommer, *J. Mater. Chem. C* **2014**, *2*, 3088.
[60] A. Luzio, D. Fazzi, D. Natali, E. Giussani, K.-J. Baeg, Z. Chen, Y.-Y. Noh, A. Facchetti, M. Caironi, *Adv. Funct. Mater.* **2014**, *24*, 1151.
[61] S. A. Jenekhe, *Adv. Mater.* **1995**, *7*, 309.
[62] R. Kim, P. S. K. Amegadze, I. Kang, H.-J. Yun, Y.-Y. Noh, S.-K. Kwon, Y.-H. Kim, *Adv. Funct. Mater.* **2013**, *23*, 5719.
[63] V. Lemaur, L. Muccioli, C. Zannoni, D. Beljonne, R. Lazzaroni, J. Cornil, Y. Olivier, *Macromolecules* **2013**, *46*, 8171.
[64] C. J. Takacs, N. D. Treat, S. Krämer, Z. Chen, A. Facchetti, M. L. Chabinyc, A. J. Heeger, *Nano Lett.* **2013**, *13*, 2522.
[65] S. M. Sze, K. K. Ng, *Physics of Semiconductor Devices*, 3rd ed., Wiley **2006**, 832.
[66] D. Boudinet, G. Le Blevennec, C. Serbutoviez, J.-M. Verilhac, H. Yan, G. Horowitz, *J. Appl. Phys.* **2009**, *105*, 084510.
[67] J.-D. Chai, M. Head-Gordon, *Phys. Chem. Chem. Phys.* **2008**, *10*, 6615.
[68] M. Cossi, N. Rega, G. Scalmani, V. Barone, *J. Comput. Chem.* **2003**, *24*, 669.
[69] M. J. Frisch, G. W. Trucks, H. B. Schlegel, G. E. Scuseria, M. A. Robb, J. R. Cheeseman, G. Scalmani, V. Barone, B. Mennucci, G. A. Petersson, H. Nakatsuji, M. Caricato, X. Li, H. P. Hratchian, A. F. Izmaylov, J. Bloino, G. Zheng, J. L. Sonnenberg, M. Hada, M. Ehara, K. Toyota, R. Fukuda, J. Hasegawa, M. Ishida, T. Nakajima, Y. Honda, O. Kitao, H. Nakai, T. Vreven, J. Montgomery, J. A. , J. E. Peralta, F. Ogliaro, M. Bearpark, J. J. Heyd, E. Brothers, K. N. Kudin, V. N. Staroverov, R. Kobayashi, J. Normand, K. Raghavachari, A. Rendell, J. C. Burant, S. S. Iyengar, J. Tomasi, M. Cossi, N. Rega, N. J. Millam, M. Klene, J. E. Knox, J. B. Cross, V. Bakken, C. Adamo, J. Jaramillo, R. Gomperts, R. E. Stratmann, O. Yazyev, A. J. Austin, R. Cammi, C. Pomelli, J. W. Ochterski, R. L. Martin, K. Morokuma, V. G. Zakrzewski, G. A. Voth, P. Salvador, J. J. Dannenberg, S. Dapprich, A. D. Daniels, Ö. Farkas, J. B. Foresman, J. V. Ortiz, J. Cioslowski, D. J. Fox, Gaussian 09, Revision D.01 **2009**.